Environmental Science and Pollution Research (2023) 30:80545–80558
https://doi.org/10.1007/s11356-023-28169-6

RESEARCH ARTICLE

Sustainable Bifunctional ZnO Composites For Synchronous Adsorption And Reduction Of Cr(VI) to Cr(III)

Nurudeen Abiola Oladoja[1] · Joseph Adebusola Ogunniyi[1] · Eric TobechukwuAnthony[1] · Sumit Kumar[2] · Stephan Hofmann[2]

Received: 21 March 2023 / Accepted: 5 June 2023 / Published online: 10 June 2023

Abstract

In decentralized systems, adsorption-based strategies offer inherent advantages for the treatment of drinking water contaminated with oxoanion. However, these strategies only involve phase transfer and not the transformation to an innocuous state. The requirement for an after-treatment procedure to manage the hazardous adsorbent further complicates the process. Here we formulate green bifunctional ZnO composites for the simultaneous adsorption and photoreduction of Cr(VI) to Cr(III). Three non-metal-ZnO composites based on raw charcoal- ZnO, modified charcoal- ZnO charcoal, and chicken feather- ZnO were prepared from the combination of ZnO with non-metal precursors. The composites were characterized and both the adsorption and photocatalyst features were studied, separately, in synthetic feedwater and groundwater contaminated with Cr(VI). The adsorption efficiency of the composites for Cr(VI) at different initial concentrations, under solar illumination without hole scavenger, and in the dark without hole scavenger, were appreciable (between 48 and 71%), and initial concentration dependent. The photoreduction efficiencies (PE%) of all the composites were > 70%, irrespective of the initial Cr(VI) concentration. The occurrence of the transformation of Cr(VI) to Cr(III) during the photoredox reaction was established. Whereas the initial solution pH value, organic load, and ionic strength had no influence on the PE (%) of all the composites, CO_3^{2-} and NO_3^- had negative impacts. The PE (%) values of the different ZnO-composites obtained for both the synthetic feedwater and groundwater systems were comparable.

Keywords Composite · Photocatalyst · Zinc Oxide · Chromium (VI) reduction · Groundwater

Introduction

As it is peculiar to the D-block elements, chromium (Cr) exists in variable oxidation states that range between + II and + VI, but only the + III and + VI are of environmental concern. At relatively low concentration, the + III variant is an essential trace element that is required for the sustenance of living being, while at high concentration, it can inhibit some metalloenzyme systems (Dubey et al. 2015). The Cr(VI), which exits as chromate (CrO_4^{2-}) in alkaline medium, and dichromate ($Cr_2O_7^{2-}$) in acidic medium, is the most toxic amongst the Cr species. It has been found as the cause of an array of liver, lung, skin and kidney conditions (Dubey et al. 2015; Saha and Orvig 2010). The International Agency for Research on Cancer (IARC) identified Cr(VI) as an important carcinogen that modulates the DNA transcription and causes significant chromosome aberration (Dubey et al. 2015; Saha and Orvig 2010).

In order to abide by the United States Environmental Protection Agency (USEPA) maximum contaminant level of 0.05 mg/L for Cr(VI) in potable water (Saha and Orvig 2010), different methods have been studied for its removal from drinking water. In small communities, adsorption-based treatment strategies are the most viable option for the treatment of oxoanion contaminated drinking water (Allaire et al. 2018). They offer high removal efficiency, simplicity, that makes it amenable for use in decentralized systems, and a high adsorbent regeneration potential (Pincus et al. 2020).

Responsible Editor: Ioannis A. Katsoyiannis

✉ Nurudeen Abiola Oladoja
bioladoja@yahoo.com; nurudeen.oladoja@aaua.edu.ng

[1] Hydrochemistry Research Laboratory, Department of Chemical Sciences, Adekunle Ajasin University, Akungba Akoko, Nigeria

[2] Department of Engineering, University of Cambridge, Cambridge, UK

Such adsorption-based approach only involves the transfer of the pollutant from one phase to another, and not the transformation from the toxic state to an innocuous state. Thus, the requirement for an after-treatment procedure to manage the hazardous pollutant laden adsorbent, which complicates the process.

In water and wastewater treatment, the transformation of toxic pollutants to the innocuous form has been explored via photocatalytic pathways. Amongst the process variables identified by Anthony and Oladoja (2022) for optimal performance of a semiconductor is the ability to provide suitable surface for the adsorption of the toxic pollutant and desorption of the transformed innocuous product formed. This salient mechanism and understanding imply that a semiconductor can be properly formulated to possess bifunctional features of an adsorbent, as well as a photocatalyst, to obviate the challenges of retaining adsorbed pollutants on the surface in the original undesirable form. In order to validate this hypothesis, we here formulate ZnO composites via a green pathway to achieve bifunctionality with adsorbent and photocatalyst features.

Considering the desirable features of ZnO semiconductor, array of its composites has been formulated and used in different applications that include sensors (Viter et al. 2020, and 2023, Turemis et al. 2020), photoelectrical devices (Wang et al. 2020a, b; Li et al. 2017; Zang 2018), and environmental remediation technologies (Dhatshanamurthi et al. 2017; Goodarzi et al. 2017; Bora et al. 2017; Anthony et al. 2020). Its use in environmental remediation technologies was ascribed to its desirable physicochemical and functional properties that include non-toxicity, high electron mobility (200–300 $cm^2\ V^{-1}\ s^{-1}$), chemical stability, and low cost (Anthony et al. 2020). Its wide band gap (3.37 eV) restricts its activity to UV light irradiation (i.e., wavelength < 387 nm) (Wang et al. 2014). In order to enable the solar activity, structural modification strategies have been developed to enhance the photon absorption and reduce the recombination rate of the photo-generated charge carriers (Bora et al. 2017). Doping ZnO with a carbonaceous material has been shown to mitigate its photocorrosion proclivity (Kumar and Rao 2015). ZnO doping with nitrogen and sulfur has been explored through different synthetic approaches (Marschall and Wang 2014). Generally, the used non-metal dopant precursors are usually expensive (e.g., graphite, activated carbon, carbon nanotubes or fullerenes), and can be toxic (e.g. most of the sulfur precursors), carcinogenic, or produce obnoxious intermediates or by-products which are not ecofriendly. In order to ensure a cost effective, sustainable and ecofriendly doping process, alternative green non-metal precursors are critically required with abundant carbon, nitrogen, and sulfur concentration.

Here, we prepared green non-metal (C, N and S) dopants from locally available resources, specifically charcoal and chicken feather, to formulate bifunctional ZnO composites for Cr(VI) adsorption, and photo-reduction to Cr(III). Charcoal, a black carbon residue, is produced from thermal decomposition of rich carbonaceous material in an inert system. Due to its highly carbonaceous nature, large surface area, and high optical absorption (black colour), charcoal has been used as filter, catalyst, adsorbent and in black pigment preparation. Chicken feather, an abundant waste product from the poultry industry, is based on the structural protein keratin (> 90%), with high content of hydrophobic residues, and cysteine (Dou et al. 2015). The chemical assay of chicken feather showed the presence of carbon (64.47%), nitrogen (10.41%), oxygen 22.34% and Sulphur (2.64%) (Tesfaye et al. 2017). We focus on the adsorption and photocatalyst features of these ZnO composites in synthetic feedwater and groundwater contaminated with Cr(VI) to evaluate their potential for Cr(VI) reduction to Cr(III) in drinking water.

Materials and methods

Material preparation and characterization

Raw charcoal (RC) was collected from a commercial bakery that uses varieties of hardwood for the generation of thermal energy, and pulverized. Modified charcoal (MC) was prepared by soaking pulverized RC in freshly prepared piranha solution (i.e., 1:3 ratio of 30% hydrogen peroxide to sulfuric acid), and then washed copiously with deionized water (electrical conductivity = 0.08 µS/cm), and then dried in the oven at 100 ± 3°C. Chicken feathers were collected from the University poultry farm, washed thoroughly with deionized water, dried at 80 °C, and then cut into small fragments. Appropriate amount of the fragmented chicken feather was soaked in warm deionized water for an hour, dried at 100 °C and then calcined in a muffle furnace at 500 °C to prepare the calcined chicken feather. The ZnO semiconductor was prepared by weighing appropriate amount of zinc acetate into a crucible with lid and then heated at 500 °C in a muffle furnace for a period of 2 h.

The non-metal-ZnO composites (i.e., raw charcoal-ZnO (RCZ), modified charcoal-ZnO (MCZ), and chicken feather ZnO (CFZ)) were prepared by stirring a mixture of the non-metal precursors with Zn acetate in a warm distilled water for 30 min., sonicate for 60 min, dry in the oven at 100 ± 3 °C and calcined in the furnace at 500 °C for 2 h.

In order to characterize the materials, the crystallinity and mineralogical assemblage were determined using X-ray diffractometer (XRD). The surface micro-structure was determined using scanning electron microscope (SEM), and the textural properties were determined using the BET methods.

The point zero charge (pH_{PZC}) values were determined using the solid addition method (Balistrieri and Murray 1981).

The photoredox reaction

The photoredox reaction was conducted in a photoreactor composed of borosilicate beakers (1.8 L, transmittance l > 280 nm), where sunlight was directed axially to the center of the reactor. With the aid of a photometer (HTC LX-101 Digital Lux Meter), the solar light intensity was quantified each time, and the average solar light intensity was 622.37W/m^2. The photoredox reaction was conducted by dissolving 0.1 g of the hole scavenger (i.e., oxalic acid) in 50 mL of Cr (VI) solution of 50 mg/L. The photocatalyst (0.1 g) was added and the mixture was agitated for 2 h before sample was withdrawn, filtered using a 0.45 µm membrane filter and the residual Cr(VI) in the filtrate was quantified using the UV/Visible spectrophotometer at $\lambda_{max} = 352$ nm (i.e., the λ_{max} of Cr(VI) in acidic medium). The photoreduction efficiency (PE%) was determined by using Eq. 1:

$$PE = \frac{[C_0 - C_f]}{C_0} \times 100 \quad (1)$$

The role of Cr(VI) adsorption by each of the composite was determined by conducting the photoredox reaction in the dark (i.e., without solar illumination) for a period of 2 h and the residual Cr(VI) concentration was determined. The influence of hole scavenger and the possible occurrence of dark catalytic reaction were determined by conducting the photoredox reaction under solar illumination but in the absence of the hole scavenger. The effect of photolysis was evaluated by conducting the photoredox reaction under solar illumination with the hole scavenger, but without the photocatalyst.

At different initial Cr(VI) concentrations (i.e., 10, 20 and 50 mg/L of Cr(VI)), the time-concentration profiles of the photoredox reaction were monitored in a reaction mixture that contained 0.1 g of photocatalyst, and 0.1 g of hole scavenger. At fixed time intervals that ranged between 0 and 120 min, samples were withdrawn, filtered using membrane filter (0.45 µm) and analyzed for the residual Cr(VI) concentrations.

The influence of reaction process variables (i.e. initial Cr(VI) solution pH, anionic interference, organic load and ionic strength) on the photoredox efficiency was determined by simulating the reaction conditions that is similitude of the groundwater matrix, viz: initial solution pH that ranged between pH 4.0 and 10.0; anionic interference by the addition of different concentrations (mg/L) (10, 50 and 100) of different anions (NO_3^-, Cl^-, and CO_3^{2-}) derived from the potassium salts; organic load, using humic acid concentration that ranged between 0 and 80 mg/L; ionic strength (tested in NaCl solutions (%): 0, 0.05, 0.1, 0.2, 0.5 and 1, equivalent to ionic strengths (mol/L) of 0, 0.0085, 0.017, 0.0342, 0.085 and 0.17).

Real life application

The PE (%) value of the three ZnO-composites were evaluated in groundwater spiked with Cr(VI) concentration of 54.1 mg/L, to evaluate the real-life application.

Results and discussion

Material characterization

The surficial architecture of the different ZnO-composite materials and the precursors are presented in Fig. 1 a-c, and the Supplementary Information file (SIFig. 1 a-c), respectively.

The SEM image of the ZnO-composites were totally different from the respective precursors, which showed that the precursors were incorporated into each other to produce new materials with a totally different surficial architecture from the respective precursors (Fig. 1 a-d). The textural properties of the composites are presented in Table 1. Both the BET surface area (m^2/g) and the t-plot external surface area (m^2/g) of the RCZ were the highest, while the MCZ had the lowest values for these two textural properties. The BET surface areas ((m^2/g) of the composite materials were in this order: RCZ (602.074) > CFZ (371.941) > MCZ (318.198). The values of the DR micropore volume (cm^3/g) and the micropore surface area (m^2/g) for the RCZ were the highest, while the MCZ had the least values (Table 1).

The diffractogram of the ZnO, (SIFig. 2 a) showed that it is a highly crystalline material and the presence of zincite (ZnO), at the following 2θ positions 31.6768, 34.2708 and 36.2247, and sphalerite (ZnS) peaks at 28.5209, 47.5738 and 56.3642 were detected. For the chicken feather (SI Fig. 2), the diffractogram showed that it is an agglomeration of both the crystalline and amorphous phases. The major minerals detected in the calcined chicken feather are quartz (SiO_2), glauconite [(K,Na) $(Fe,Al,Mg)_2$. $(Si,Al)_4$. O_{10}. $(OH)_2$] and albite ($NaAlSi_3O_8$). The detailed mineralogical assemblage of both the raw and modified charcoal have been presented in another treatise, but highlighted here for brevity. In the RC, two major peaks attributed to calcite ($CaCO_3$) and Whewellite, ($C_2CaO_4 \cdot H_2O$/$CaC_2O_4 \cdot H_2O$) were observed. In the MC, the modification procedure enhanced the crystallinity phase of the material, while the disappearance of the two major peaks identified in the RC were observed. In the MC, two new peaks that are synonymous with anhydrite, ($CaSO_4$) and graphite were observed.

The mineralogical assemblage and the crystallinity of the ZnO-composites (Fig. 2 a-c) showed that the composites are

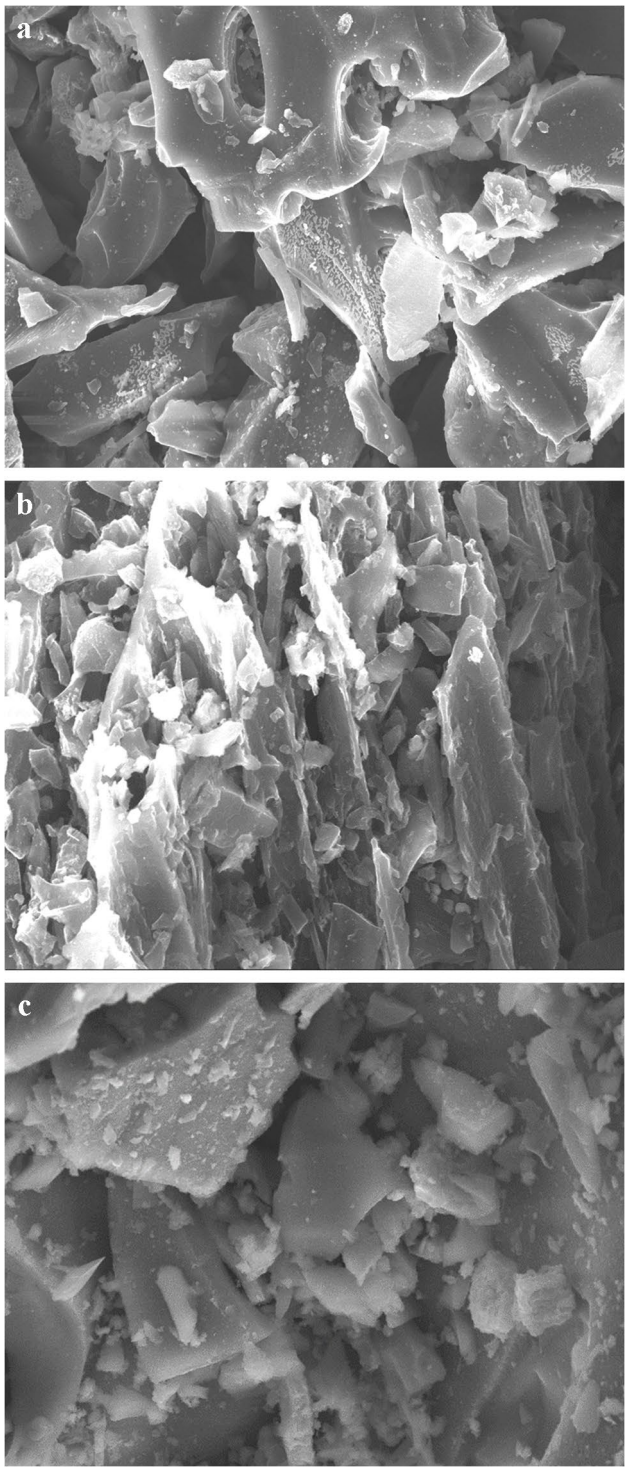

Fig. 1 **a** The SEM image of RCZ composite, **b** The SEM image of MCZ composite, **c** The SEM image of CFZ composite

mosaic of amorphous and crystalline phases. The diffractograms presented in Fig. 2 b-d showed the prominence of zincite peaks at 2θ values of 31.85◦, 34.46◦, 36.26◦ and 47.61◦, while the presence of other zinc minerals (e.g., sphalerite and zinc) were also detected. Considering the prominence of the ZnO crystalline peaks, it could be inferred that the semiconductor constituent is the major crystalline phase of the composite.

Table 1 The textural properties of the composite materials

Parameters	RCZ	MCZ	CFZ
i) BET Surface Area(m^2/g)	602.07	318.20	371.94
ii) t-Plot external surface area	602.07	318.20	371.94
iii) DR Micropore volume (cm^3/g)	0.24	0.11	0.15
iv) Average Pore width (nm)	6.30	6.67	6.03
v) Adsorption energy (kJ/mol)	4.13	3.90	4.31
vi) DR Micropore surface area (m^2/g)	667.83	309.91	411.44
vii) DFT cumulative Pore volume (cm^3/g)	0.18	0.08	0.11
viii) DA Pore Diameter (nm)	2.92	3.04	2.88

The result of the pH_{PZC} for the different composites are presented in the SIFig. 3 a-c, and the pH_{PZC} values for RCZ was 8.3, MCZ was 7.2 and CFZ was 8.1.

Determination of Cr(VI) removal efficiency

The role of adsorption in Cr(VI) removal

The adsorption efficiencies of the precursors that constitute the composites for Cr(VI) was determined at a fixed Cr(VI) concentration (50 mg/L) and agitation time (2 h). The MC exhibited the highest affinity for Cr(VI), with adsorption efficiency of 17.52 mg/g (i.e., 70.5% removal), while the other precursors (i.e., CF, RC and ZnO) showed poor affinity for Cr(VI), each with less than 5% removal efficiency.

The adsorption efficiencies of the composites (i.e., MCZ, RCZ and CFZ) for Cr(VI) at different initial Cr(VI) concentrations that ranged between 10 and 50 mg/L and fixed time (2 h) were investigated under solar illumination, and in the dark, each without the hole scavenger. The time-concentration profiles of the adsorption of Cr(VI) from aqueous solution using the different ZnO-composites are presented in SI Fig. 4 a-f. In both cases (i.e. in the dark and under solar illumination without hole scavenger), appreciable amount of the Cr(VI) was removed and the percentage Cr(VI) removal, which was initial concentration dependent, ranged between 48 and 71%. The amount of Cr(VI) removed per gram of the composite material (q_e mg/g) increased with increasing initial Cr(VI) concentration (SI Fig. 4 a-f). In order to evaluate the rate of adsorption and other rate dependent parameters, under the two reaction conditions, the time-concentration-profile data, obtained at different initial Cr(VI) concentrations, were analyzed with pseudo first order and pseudo second order kinetic Equations.

The pseudo first order Equation (Eq. 1), which describes liquid–solid phase adsorption systems is the earliest known

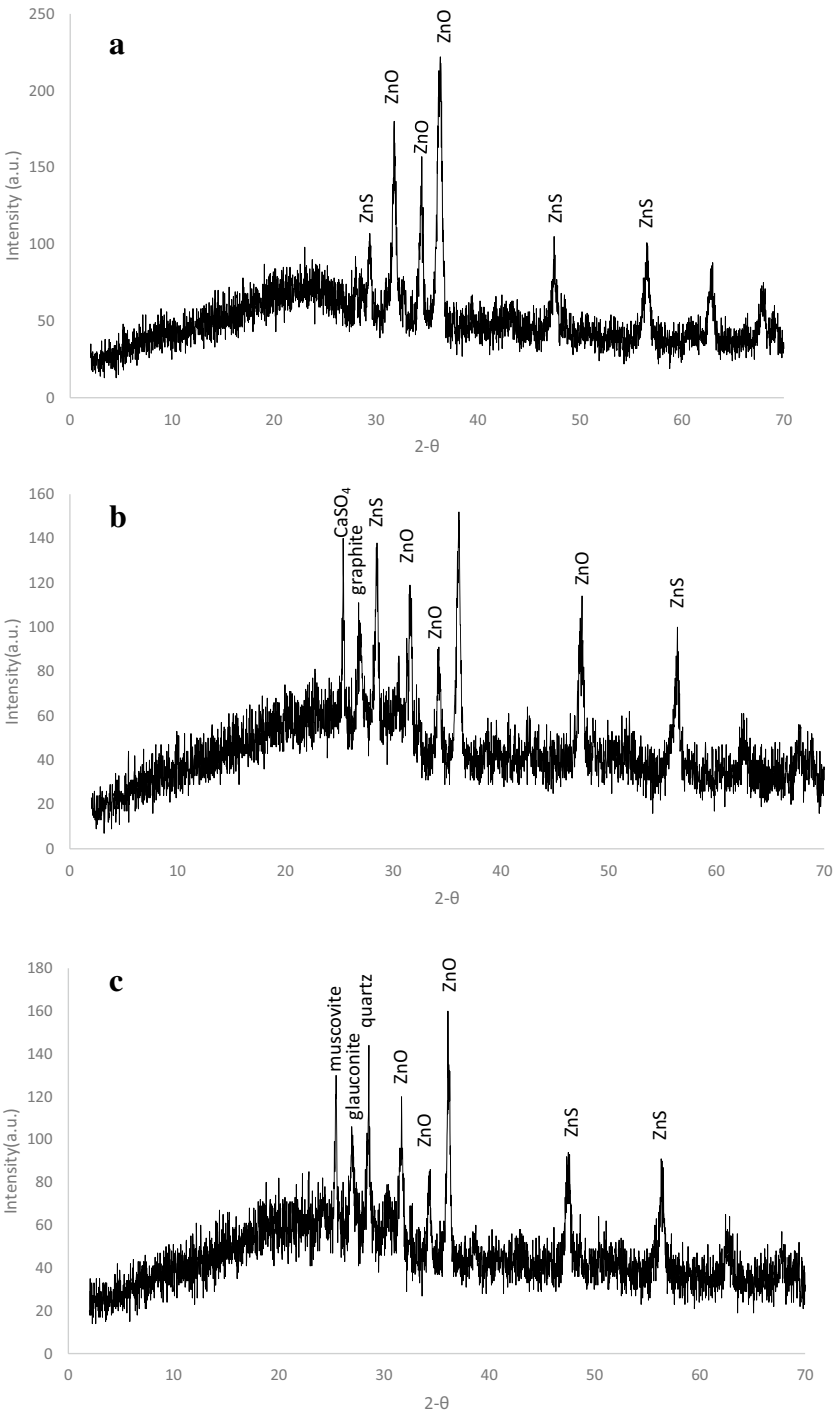

Fig. 2 **a** The X-ray diffractogram of the RCZ composite, **b** The X-ray diffractogram of the MCZ composite, **c** The X-ray diffractogram of the CFZ composite

kinetic equation that provided insight into the adsorption rate based on the adsorption capacity (Lagergren 1898).

$$\log\left(q_e - q_t\right) = \log\left(q_e\right) - \frac{k_1}{2.303}t \tag{1}$$

where, q_e and q_t are the adsorption capacity at equilibrium and at time, t, respectively (mg/g). k_1 is the rate constant of pseudo first-order adsorption.

The pseudo-second-order kinetic equation (McKay 1984) (Eq. 2) describe chemisorption as well as ion exchange reaction mechanisms.

$$\frac{t}{q_t} = \frac{1}{kq_e^2} + \frac{1}{q_e}t \tag{2}$$

where, q_e, q_t, and t have the same meaning as explained above and k_2 is the overall rate constants of pseudo-second-order sorption (g(mg/min)).

The results of the kinetic analysis (Tables 2 and 3) showed that the pseudo-second-order kinetic equation fitted the process of Cr(VI) adsorption by the composites better ($r^2 > 0.99$) than the pseudo first order kinetic equation ($r^2 < 0.93$). The pseudo second order equilibrium sorption capacity, q_e, and the overall rate constant of pseudo second (k_2) parameter increased with increasing initial Cr(VI) concentrations. At initial Cr(VI) concentration (mg/L) that ranged between 10.25 and 54.42: the q_e(mg/g) values ranged between 3.67 and 18.21 for MCZ, 2.53 and 17.61for RCZ, and 2.67 and 17.67 for CFZ; the values of k_2 (g(mg/min)) ranged between 0.29 and 10.56 for MCZ, 0.45 and 18.93 for RCZ, and 0.43 and 19.52 for CFZ. The better fitting of the pseudo second order kinetic equation to the time-concentration profile data is an indication that the adsorption of Cr(VI) by the different composites occurred via chemisorption or ion exchange mechanism.

The photoredox reaction

The photoreduction efficiencies (PE%) of the ZnO-composites were evaluated under solar illumination. At an initial Cr(VI) concentration of 53.17 mg/L, the PE% values were 90.54 for MCZ, 85.18 for RCZ and 86.13 for CFZ under solar illumination. In the dark, (i.e., without solar illumination) the PE (%) values obtained were 66.96 for MCZ, 64.73 for RCZ and 64.88 for CFZ. The results obtained from these studies showed that the contribution of adsorption to the PE (%) was significant, and the synergistic effects of both photoredox reaction and adsorption underlie the process of Cr(VI) attenuation in the synthetic feedwater system during

Table 2 Kinetic parameters of the Cr(VI) adsorption process in the dark

	Pseudo 1st order parameters			Pseudo 2nd order parameters		
Initial Conc. (mg/L)	q_{e1} (mg/g)	K_1 (g/(mg min)	R^2	q_{e2} (mg/g)	K_2 (g/(mgmin))	R^2
MCZ						
10.25	1.44	0.0316	0.957	3.67	0.2931	0.9969
20.94	3.02	0.0352	0.8976	7.22	0.2616	0.9947
54.42	5.26	0.0147	0.9016	18.21	10.5577	1.000
RCZ						
10.25	1.28	0.0355	0.966	2.53	0.4534	0.999
20.94	2.75	0.0461	0.9719	5.90	0.2756	0.9967
54.42	5.26	0.0316	0.6405	17.61	18.9333	1.000
CFZ						
10.25	1.09	0.0451	0.9845	2.67	0.4248	0.9988
20.94	2.41	0.0283	0.9466	6.10	0.2527	0.9954
54.42	7.79	0.0263	0.9628	17.67	19.5172	1.000

Table 3 Kinetic parameters of the Cr(VI) adsorption under solar illumination without hole scavenger

	Pseudo 1st order parameters			Pseudo 2nd order parameters		
Initial Conc. (mg/L)	q_{e1} (mg/g)	K_1 (g/(mg min)	r^2	q_{e2} (mg/g)	K_2 (g/(mgmin))	r^2
MCZ						
10.89	1.79	0.0276	0.9532	3.97	0.1967	0.9919
19.63	3.25	0.0313	0.9532	6.93	0.2140	0.9938
51.08	1.40	0.0164	0.7242	16.92	3.3771	0.9999
RCZ						
10.89	1.07	0.0426	0.9985	2.89	0.4673	0.9993
19.63	3.62	0.0322	0.9341	5.94	0.1410	0.9868
51.08	1.08	0.0502	0.8667	16.50	4.3913	1.0000
CFZ						
10.89	1.03	0.0373	0.9682	3.04	0.4213	0.9999
19.63	3.69	0.0439	0.9331	6.10	0.1821	0.9938
51.08	1.52	0.0408	0.8905	16.58	5.6887	1.0000

the photoredox reaction. The synergistic effect was induced by the favourable adsorptive surface created by the ZnO-composites, which promoted the adsorption of Cr(VI) for the subsequent occurrence of photoredox reaction.

The influence of the different constituents of the reacting mixture (i.e., the photocatalyst and the hole scavenger) on the PE (%) was evaluated by conducting the photoredox reaction under solar light illumination, with and without the hole scavenger, and with the hole scavenger alone but without the photocatalyst. The PE (%) exhibited by the different ZnO-composite photocatalyst was 66.45% for MCZ, 64.55% for RCZ, and 64.87% for CFZ, without the hole scavenger. The PE(%) in the presence of hole scavenger, without the photocatalyst, was 7.88%, which accounted for the poor effect of photolysis on the Cr(VI) reduction. The removal of Cr(VI) in the presence of the hole scavenger alone, sunlight illumination, and without the ZnO-composite, was negligible despite the fact that the hole scavenger used (i.e. oxalic acid) has been reported to be sacrificial donor (i.e. a reducer) (Mytych et al. 2005).

The UV–visible spectra that shows the time-concentration profiles of the photoreduction of Cr(VI) by the photocatalysts are presented in Fig. 3 a-c. The plot of the time-concentration profiles at different initial Cr(VI) concentration (i.e., 9.77, 22.43, and 53.17 mg/L) are presented in Fig. 4 a-c. The value of the PE (%) reduced with increasing initial Cr(VI) concentration, and the MCZ composites gave higher PE (%) values than the other two composites at the different initial Cr(VI) concentrations (Table 4).

At the lowest initial Cr(VI) concentration (i.e., 9.77 mg/L), the PE(%) values for the different ZnO-composites ranged between 88.70 and 95.04, while at the highest initial Cr(VI) concentration (i.e., 53.17 mg/L), the PE(%) values ranged between 85.18 and 90.54. The process rate parameters, derived from the fitting of the time-concentration profile data to the pseudo first order kinetic Equation (Eq. 2), at the different initial Cr(VI) concentrations are as presented in Table 4.

The corresponding half-lives ($t_{1/2}$) values were calculated using Eq.3 .

$$\ln\frac{\left[Cr(VI)_0\right]}{[Cr(VI)]} = k_{red}t \tag{2}$$

$$t_{1/2} = \frac{ln2}{k_{red}} \tag{3}$$

The k_{red} value was calculated from slope of the plot of ln (C_0/C) versus time (t), where C_0 and C denote the Cr(VI) concentrations at t = 0 and t = t, respectively, $t_{1/2}$ stands for the half-lives of Cr(VI) reduction.

Premised on the values of the r^2 obtained (> 0.9) at the different initial Cr(VI) concentration, the pseudo first order kinetic Equation fitted the time-concentration profiles of the photoreduction process (Table 4). While the k_{red} values reduced with increasing initial Cr(VI) concentrations, a reverse in trend was observed with the half-lives ($t_{1/2}$) of Cr(VI) reduction (Table 1). The dependency of the K_{red} values on the initial Cr(VI) concentration was ascribed to the rate of reaction and magnitude of the reactive species generated on the photocatalyst surface. The extent of interaction between these active reactive species and the aqueous phase Cr(VI) oxoanion at the different initial Cr(VI) concentration is also a factor (Konstantinou and Albanis 2004). At higher initial Cr(VI) concentration, the propensity of the ZnO-composite photocatalyst to generate active radicals is inhibited because the Cr(VI) occupies more adsorptive sites on the photocatalyst surface. It has also been postulated (Konstantinou and Albanis 2004) that at higher initial substrate concentrations, significant absorption of the irradiated light by the substrate molecules occurs in the aqua matrix, rather than the absorption by the photocatalyst, thereby retarding the photoreduction efficiency. Thus, the magnitude of both the photoinduced electron–hole pairs and their corresponding oxygen active radicals are significantly reduced at this higher substrate concentration.

In order to establish the occurrence of the transformation of Cr(VI) to Cr(III) during the photoredox reaction, the conversion of Cr(VI) to Cr(III) under solar illumination, with hole scavenger, was evaluated using a simple qualitative test that include the addition of excess sodium hydroxide solution to the treated water obtained from the photoreduction reactions (Celebi et al. 2017; Badhe et al. 2018). After the photoredox reaction, the aqueous solution was treated with an excess amount of NaOH solution with and without heating. The change in colour of the treated water containing Cr(III) to a light-greenish colour was observed (Fig. 5 (***3***)). In the second qualitative test for the detection of the presence of Cr (III), the mixture was heated after the addition of NaOH and the solution turned greenish due to the formation of hexahydroxochromate (III) (Fig. 5 (***4***)).

The effects of process variables on the photoreduction process

Since the aqueous system pH value influences the charge on the photocatalyst particles, size of catalyst aggregates and the positions of the conductance and the valence bands (Chong et al. 2010), the influence of the initial solution pH value on the PE (%) values were evaluated between the initial Cr(VI) solution pH of 4 and 10. Within these initial solution pH values studied, the solution pH value had minimal effects on the PE (%) values of the MCZ, while no effects was observed for the other two composites (Fig. 6). For the MCZ, the PE values slightly reduced from a value of 94% at the lowest pH value (4.22), to a value of

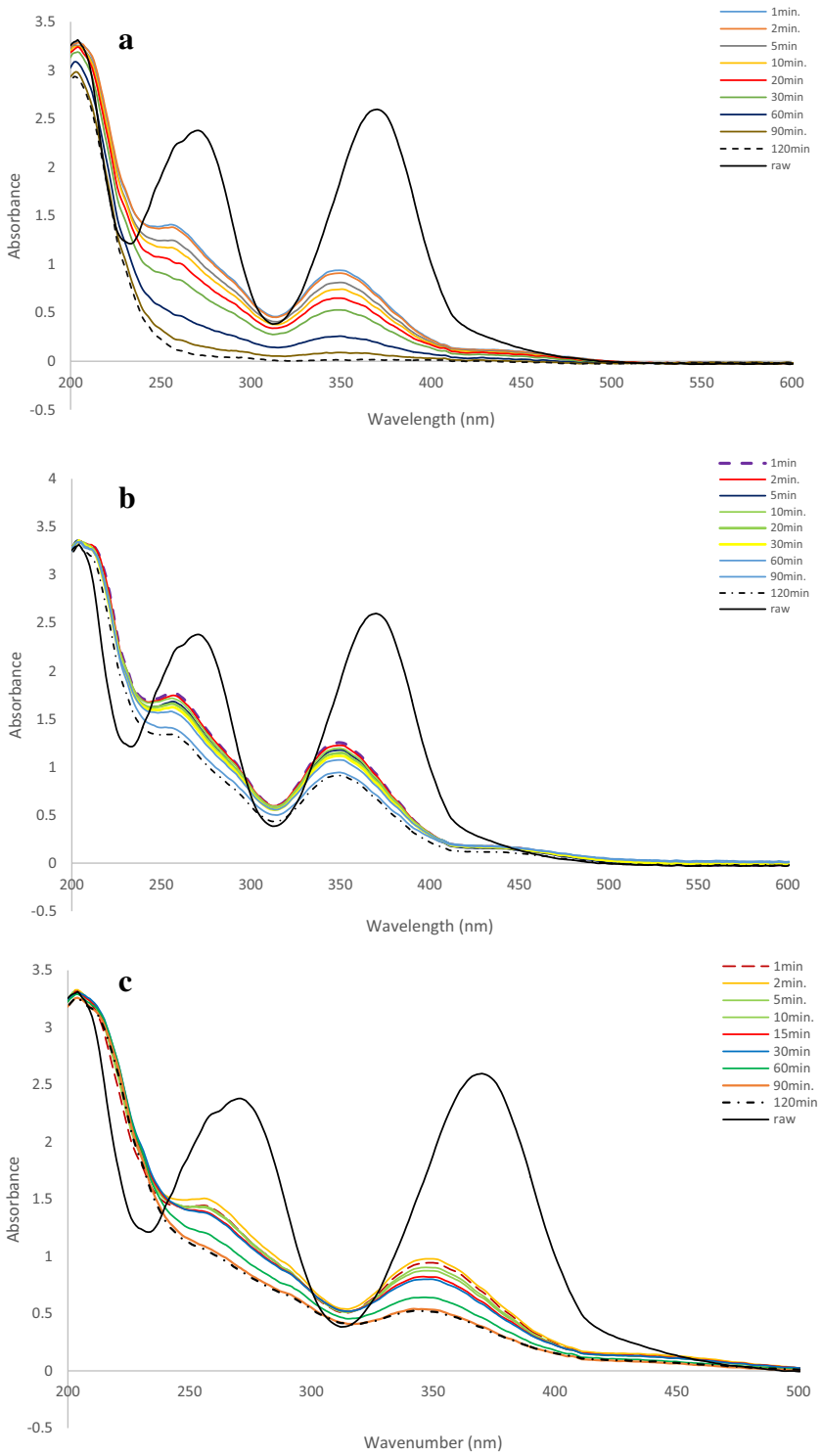

Fig. 3 **a** Time-concentration profiles of the photoreduction of Cr(VI) using MCZ composite, **b** Time-concentration profiles of the photoreduction of Cr(VI) using RCZ composite, **c** Time-concentration profiles of the photoreduction of Cr(VI) using CFZ composite

86% at the highest initial pH value (10.06). The determination of the final pH value after the photoreduction process showed that the added constituents of the reacting mixture (i.e., the hole scavenger and the photocatalyst) altered the operating pH value. While the initial solution pH values of the Cr(VI) solution ranged between 4 and 10, the final pH values ranged between 2 and 5.

The elucidation of the pH dependent Cr(VI) speciation, using the hydrochemical equilibrium data of Cr(VI) in MEDUSA (Make Equilibrium Diagrams Using

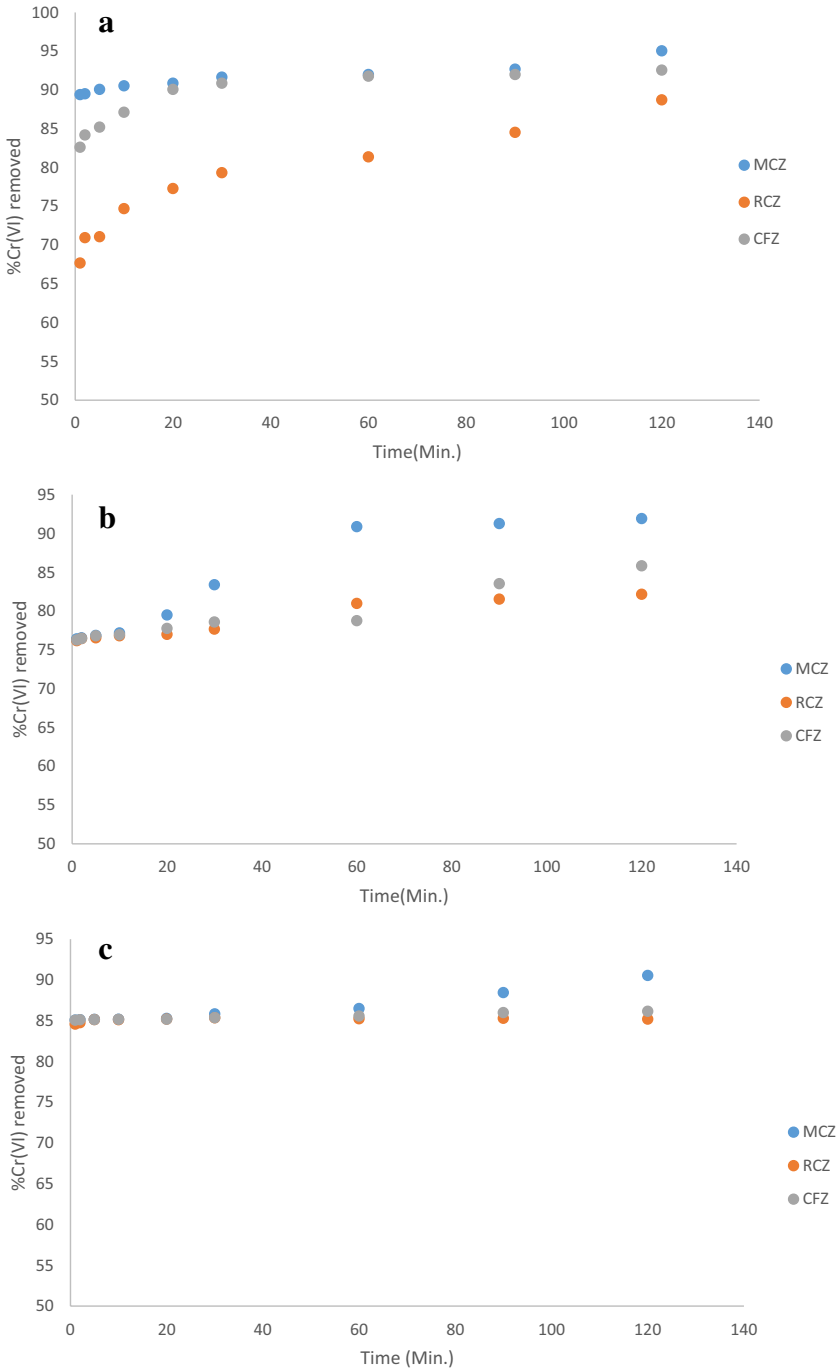

Fig. 4 Time-concentration profiles of the photoreduction of Cr(VI) @ different initial Cr(VI) concentrations (**NB**: **A** = 9.77 mg/L, **B** = 22.43 mg/L and **C** = 53.17 mg/L)

Sophisticated Algorithms) and HYDRA (Hydrochemical Equilibrium Constant Database) software (http://www.kemi.kth.se/medusa/) showed that the Cr(VI) exist in the following forms: $HCrO_4^-$; $Cr_2O_7^{2-}$; H_2CrO_4 (@ pH ≤ 6.627) and CrO_4^{2-} (@ pH > 6.627). Considering the final pH value of the reacting mixture, which ranged between the values of 2 and 5, it could be posited that the limited influence of the varying initial solution pH value could be attributed to the similarities in the aqueous phase Cr(VI) species, within the operating pH window.

Amongst the anionic interference investigated, only the presence of carbonate (CO_3^{2-}) and nitrate (NO_3^-) vitiated the PE (%) value in both the MCZ and RCZ (Fig. 8), while only CO_3^{2-} negatively impacted the PE (%) in the CFZ composite. The impact of the interfering anions increased with increasing anionic species concentration (Fig. 8). The negative impacts of these interfering anions could be ascribed to the fact that these two anionic species are also susceptible to being photo reduced by the ZnO-composites, which placed them in competitive position with

Table 4 Photoreduction efficiency and first-order rate parameters of Cr(VI) reduction

Initial Cr(VI) Conc. (mg/L)	PE(%)	K_{red} $(min.^{-1}) \times 10^{-2}$	$t_{1/2}$	r^2
MCZ				
9.77	95.04	0.0053	130.78	0.9167
22.43	91.90	0.0104	66.65	0.9135
53.17	90.54	0.0035	198.04	0.9262
RCZ				
9.77	88.70	0.0077	90.02	0.953
22.43	82.16	0.0027	256.72	0.9462
53.17	85.18	0.0002	3465.74	0.2827
CFZ				
9.77	92.55	0.0065	106.64	0.7396
22.43	85.83	0.0041	169.06	0.9368
53.17	86.13	0.0007	990.21	0.9845

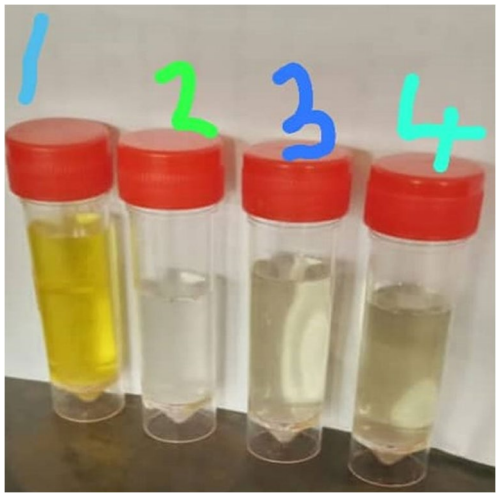

Fig. 5 Qualitative determination of the photoreduction of Cr(VI) to Cr(III) via the formation of dark green hexahydroxochromate ($[Cr(OH)_6]^{3-}$) solution by addition of excess NaOH (**1** = raw Cr(VI) solution; **2** = treated Cr(VI) solution; **3** = NaOH added at room temperature; **4** = heated after the addition of NaOH)

Cr(VI) during the photoreduction process. Considering the operating solution pH value range (pH<7), the existence of all the CO_3^{2-} species is feasible in the Cr(VI) solution but the species that predominates are H_2CO_3, HCO_3^- and CO_2. These carbonate species are susceptible to photoreduction to different organic species (e.g., HCOOH, HCHO, CH_3OH CH_4 and CH_3OH) and carbon (II) oxide (CO). For the NO_3^-, a sequential reduction to nitrogen gas is also possible. Thus, the synchronous photoreduction of Cr(VI) and the interfering aqua phase CO_3^{2-} and NO_3^- species caused a negative impact on the overall PE (%) of the Cr(VI) to Cr(III) (Fig. 7).

The difference in the ionic strength of the reacting mixture had no visible impact on the PE (%) of the composites (Fig. 8). Despite the variation in the ionic strength of the Cr(VI) solution from a value of 0.05 mol/L to 1 mol/L, the PE (%) values ranged between 87 and 95% for all the composite. The influence of organic load, simulated with humic acid, had no appreciable impact on the PE (Fig. 9). Irrespective of the initial HA concentration, the PE (%) values were at par with the system spiked with 0% HA.

Performance efficiencies of composites in groundwater system

The PE (%) value of the three ZnO-composites were evaluated in groundwater spiked with Cr(VI) concentration of 54.1 mg/L. Although, a slight decrease in the PE (%) values of the different ZnO-composites were obtained in the groundwater system, but the PE (%) values were comparable with what obtained in the synthetic feedwater system at 53.17 mg/L Cr(VI)) concentration. In the groundwater system, the PE(%) values obtained were 90.3 for MCZ, 71.0 for RCZ and 79.0 for CFZ, while in the synthetic feed water system, the PE (%) values were 90.5 for MCZ, 85.2 for RCZ, and 86.1 for CFZ. The slight decrease in the PE(%) values of the composites in the groundwater system could be

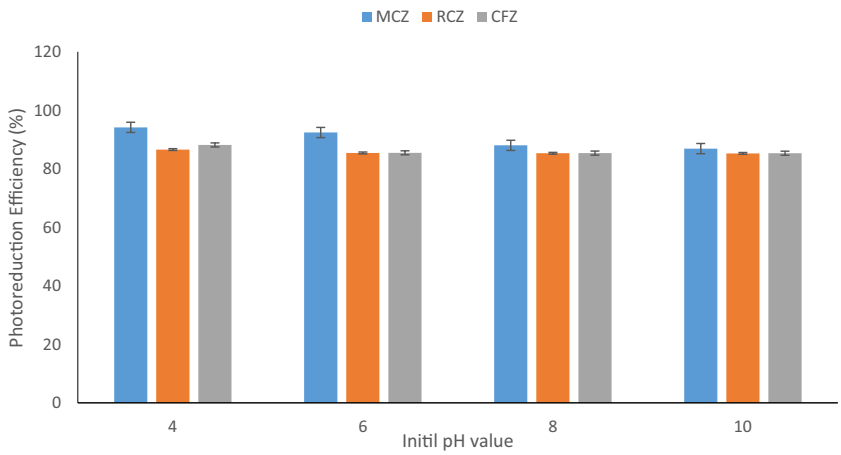

Fig. 6 Effect of initial solution pH value on the photoreduction efficiencies (%) of the composites

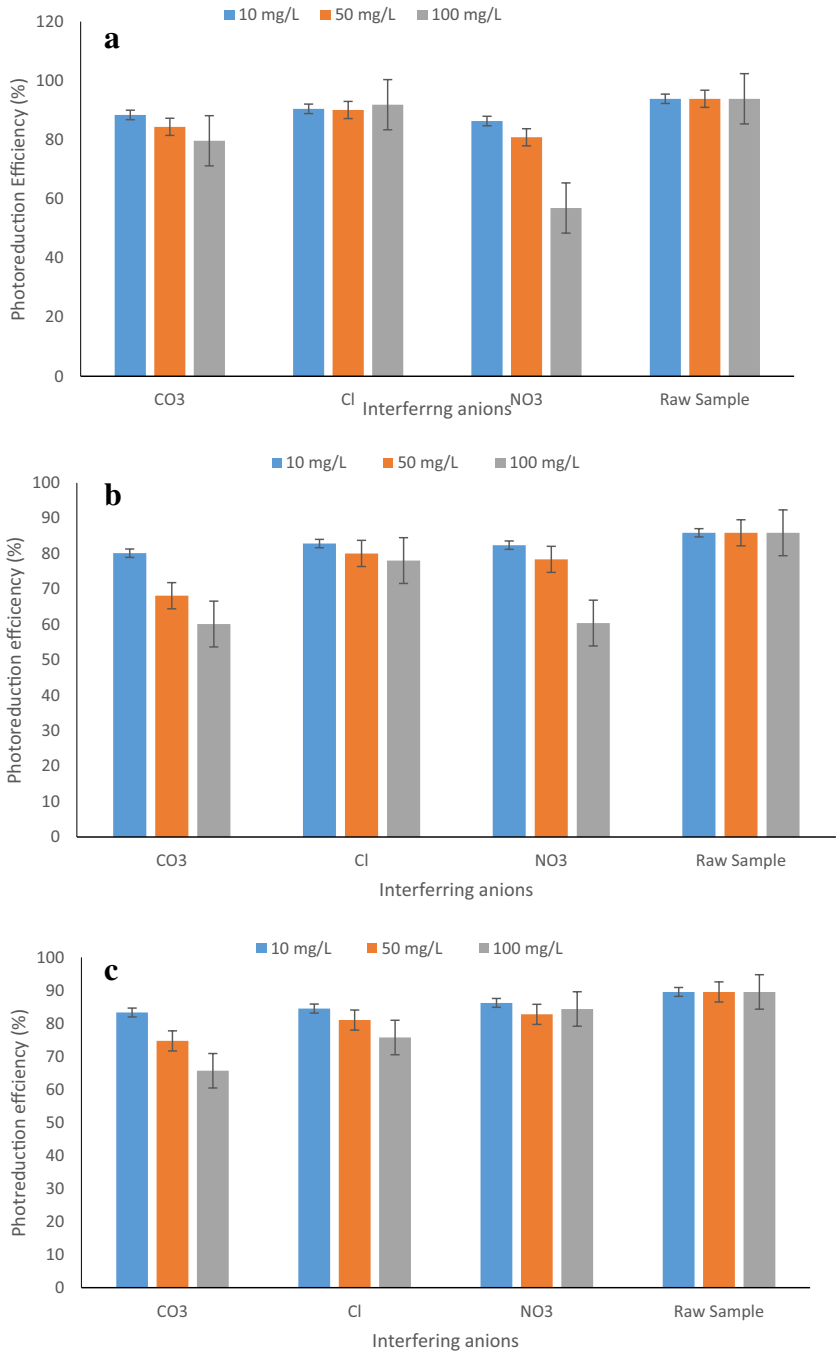

Fig. 7 Influence of anionic interference on the photoreduction efficiencies (%) of the composites (**A** = MCZ, **B** = RCZ, **C** = MCZ)

attributed to the multicomponent nature of the groundwater, which created an antagonistic effect on the photoredox process. The antagonistic effects of the presence of CO_3^{2-} and NO_2^- on the PE (%) values of the composites were affirmed when the effects of interfering anionic species were evaluated (Fig. 7).

The evaluation of the effects of the photoredox process on the physicochemical characteristics of the treated water showed that the pH value of the treated water was negatively impacted by the photoreduction process (Fig. 10). While the pH value of the groundwater spiked with Cr(VI) was 6.5, the trend in the pH values of the treated with the different composites were 3.4 for MCZ, 3.3 for RCZ, and 2.7 for CFZ. The significant decrease in the pH value of the treated water could be attributed to the acidic hole scavenger (i.e., the oxalic acid) added to the reacting mixture.

The comparison of the electrical conductivity (EC µs/cm) of the groundwater spiked with Cr(VI), with that of the

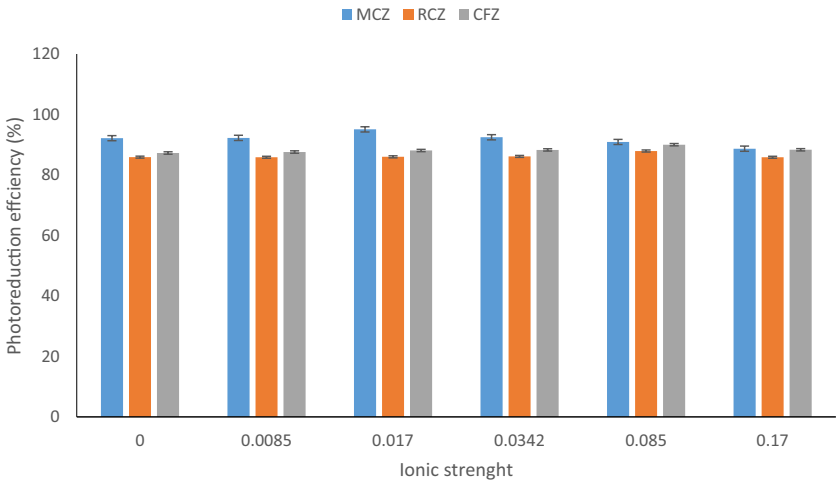

Fig. 8 Effect of solution ionic strength on the photoreduction efficiencies (%) of the composites

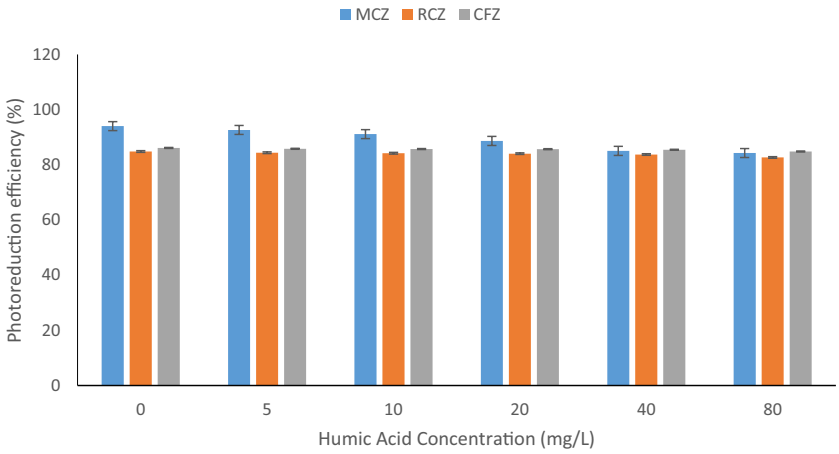

Fig. 9 Effect of organic load on the photoreduction efficiencies (%) of the composites

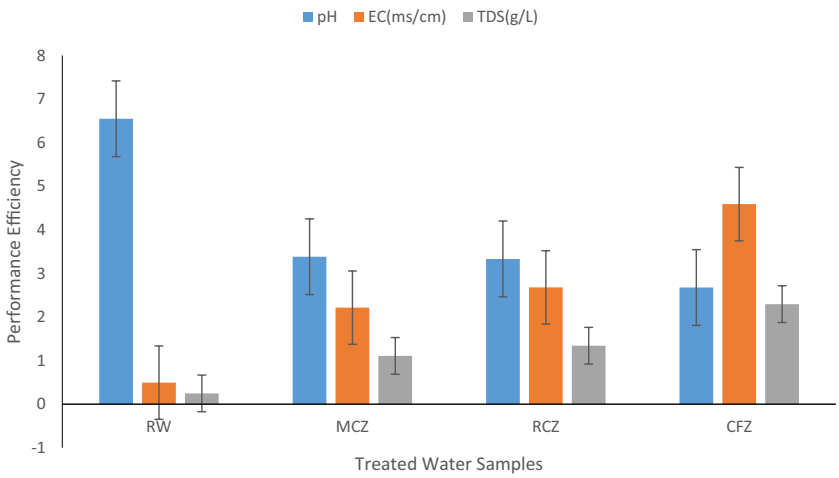

Fig. 10 Comparison of the physicochemical characteristics of treated and untreated groundwater spiked with Cr (VI)

treated water using the three ZnO-composites showed that the photoreduction process had significant impact on the ionic constituents of the treated water. The EC (ms/cm) of the raw groundwater spiked with Cr(VI) (at 54.15 mg/L) was 0.4926 (ms/cm), while the EC (ms/cm) values for the treated waters were 2.215 (MCZ), 2.678(RCZ) and 4.588(CFZ). The astronomical increase in the EC values could be ascribed to the leaching of inorganic ionic species from the photocatalyst composites into the water matrix, which induced the substantial EC (µs/cm) increase. An evaluation of the

TDS (g/L) showed a similar trend in the value with that of the EC (ms/cm) values. A significant increase in the TDS (g/L) value was observed, when compared with the untreated raw GW spiked with Cr(VI) (TDS = 0.25 g/L), and the CFZ produced treated water with the highest TDS (2.3 g/L) value, while the MCZ produced water with the lowest TDS (1.1 g/L) value. The increase in the TDS value was attributed to the possible leaching of some of the constituents of the photocatalysts into the treated water matrix, which also impacted the values of the EC (ms/cm).

Conclusion

The comparison of the surficial architecture of the different ZnO-composite materials with the precursors showed that the precursors were incorporated into each other to produce new materials with different surficial architecture from the precursors. The mineralogical assemblage and the crystallinity of the ZnO-composites showed that the composites are mosaic of amorphous and crystalline phases. The contribution of adsorption to the PE (%) was significant, and the synergistic effects of both photoredox reaction and adsorption underlie the process of Cr(VI) attenuation in the synthetic feedwater system. Although, a slight decrease in the PE (%) values of the different ZnO-composites were obtained in the groundwater system, but the PE (%) values were comparable with what obtained in the synthetic feedwater system at 53.17 mg/L Cr(VI)) concentration. Some of the physicochemical characteristics (e.g., pH, EC, TDS) of the treated groundwater using the ZnO-composites were negatively impacted to different degrees. Considering the promising performance efficiencies exhibited by the different ZnO composites prepared, it is recommended that the method of synthesis should be optimised for optimal performance, and to preclude some of the challenges identified with the treatment of the Cr(VI) spiked groundwater. A microcosm comprehensive real-life study should be conducted to enable the derivation of the process operational parameters for field applications.

Supplementary Information The online version contains supplementary material available at https://doi.org/10.1007/s11356-023-28169-6.

Acknowledgements The Authors are grateful to the Cambridge-Africa ALBORADA Research Fund (RG86330), for the grant awarded to N. A. Oladoja to collaborate with S. Hofmann to undertake this research.

Authors' contribution Oladoja, N. A. conceptualized the research, sourced for funding, supervised the research, wrote the manuscript and submitted the manuscript.

Ogunniyi, J. A. performed the experiment, and compiled the data.

Anthony, E. T. analyzed and validated the data.

Kumar, S. involved in experimental design, and edited the manuscript draft.

Hofmann, S. involved in experimental design, sourced for funding, and revised the manuscript draft.

Funding Cambridge-Africa ALBORADA Research Fund.

Data availability Not applicable.

Declarations

Ethical approval Not applicable.

Consent to participate All authors read and approved the final manuscript.

Consent to publish Not applicable.

Competing interest The author(s) declared no potential conflicts of interest to the authorship and publication of this article.

References

Allaire M, Wu H, Lall U (2018) National Trends in Drinking Water Quality Violations. Proc 805 Natl Acad Sci 115(9):2078–2083. https://doi.org/10.1073/pnas.1719805115

Anthony ET, Oladoja NA (2022) Process enhancing strategies for the reduction of Cr(VI) to Cr(III) via photocatalytic pathway. Environ Sci Pollut Res 29(6):8026–8053. https://doi.org/10.1007/s11356-021-17614-z

Anthony ET, Lawal IA, Bankole MO, Klink M, Ololade IA, Oladoja NA (2020) Solar active heterojunction of p-CaFe2O4/n-ZnO for photoredox reactions. Environ Technol Innov 20:101060

Badhe RA, Ansari A, Garje SS (2018) One-Pot Synthesis of Pd-Based Ternary Pd@CdS@TiO2 Nanoclusters via a Solvothermal Route and Their Catalytic Reduction Efficiency toward Toxic Hexavalent Chromium. ACS Omega 3:18663–18672

Balistrieri LS, Murray JW (1981) The surface chemistry of goethite (α-FeOOH) in major ion seawater. Am J Sci 281(6):788–806

Bora T, Sathe P, Laxman K, Dobretsov S (2017) Dutta, Defect engineered visible light active ZnO nanorods for photocatalytic treatment of water. J Catalysis Today 284(15):11–18

Celebi M, Karakas K, Ertas IE, Kaya M, Zahmakiran M (2017) Palladium Nanoparticles Decorated Graphene Oxide: Active and Reusable Nanocatalyst for the Catalytic Reduction of Hexavalent Chromium (VI). ChemistrySelect 2:8312–8319

Chong MN, Jin B, Chow CWK, Saint C (2010) Recent developments in photocatalytic water treatment technology: A review. Wat Res 44:2997–3027

Dhatshanamurthi P, Shanthi M, Swaminathan M (2017) An efficient pilot scale solar treatment method for dye industryeffluent using nano-ZnO, Journal of Water. Process Eng 16:28–34

Dou Y, Huang X, Zhang B, He M, Yin G, Cui Y (2015) Preparation and characterization of a dialdehyde starch crosslinked feather keratin film for food packaging applications. RSC Adv 5:27168–27174

Dubey R, Bajpai J, Bajpai AK (2015) Green synthesis of graphenes and composite (GSC) as novel adsorbent for efficient removal of Cr(VI) ions from aqueous solution. J Water Process Eng 5:83–94

Goodarzi M, Joukar S, Ghanbari D, Hedayati K (2017) CaFe2O4–ZnO magnetic nanostructures: photo-degradation of toxic azo-dyes under UV irradiation. J Mater Sci: Mater Electron 28:12823–12838

Konstantinou IK, Albanis TA (2004) TiO_2-assisted photocatalytic degradation of azo dyes in aqueous solution: kinetic and mechanistic investigations: a review. Appl Catal b: Environ 19:1–14

Kumar SG, Rao KSRK (2015) Zinc oxide based photocatalysis: tailoring surface-bulk structure and related interfacial charge

carrier dynamics for better environmental applications. RSC Adv 5:3306–3351
Lagergren S (1898) About the theory of so-called adsorption of soluble substances. K Sven Vetenskapsakad Handl Band 24:1–39
Li C, Zang Z, Han C, Hu Z, Tang X, Du J, Leng Y, Sun K (2017) Highly compact CsPbBr 3 perovskite thin films decorated by ZnO nanoparticles for enhanced random lasing. Nano Energy 40:195–202
Marschall R, Wang L (2014) Non-metal doping of transition metal oxides for visible-light photocatalysis. Catal Today 225:111–135
McKay G (1984) The adsorption of basic dye onto silica from aqueous solution-solid diffusion model. Chem Eng Sci 39(1):129–138
Mytych P, Ciesla P, Stasicka Z (2005) Photoredox processes in the Cr(VI)–Cr(III)–oxalate system and their environmental relevance. Appl Catal B 59:161–170
Pincus L, Rudel H, Petrovic P, Gupta S, Westerhoff P, Muhich C, Zimmerman JB (2020) Exploring the Mechanisms of Selectivity for Environmentally Significant Oxo-anion Removal During Water Treatment: A Review of Common Competing Oxo-anions and Tools for Quantifying Selective Adsorption, https://doi.org/10.1021/acs.est.0c01666 • Publication Date (Web)
Saha B, Orvig C (2010) Biosorbents for hexavalent chromium elimination from industrial and municipal effluents. Coord Chem Rev 254:2959–2972
Tesfaye T, Sithole B, Ramjugernath D, Chunilall V (2017) Valorization of chicken feathers: characterization of chemical properties. Waste Manag 68:626–635
Turemis M, Zappi D, Giardi MD, Basile G, Ramanaviciene A, Kapralovs A, Ramanavicius A, Viter R (2020) ZnO/Polyaniline Composite Based Photoluminescence Sensor for the Determination of Acetic Acid Vapor. Talanta 211:120658
Viter R, Kunene K, Genys P, Jevdokimovs D, Erts D, Sutka A, Bisetty K, Viksna A, Ramanaviciene A, Ramanavicius A (2020) Photoelectrochemical bisphenol S sensor based on ZnO-nanoroads modified by molecularly imprinted polypyrrole. Macromol Chem Phys 221:1900232
Viter R, Fedorenko V, Gabriunaite I, Tepliakova I, Ramanavicius S, Holubnycha V, Ramanavicius A, Valiūnienė A (2023) Electrochemical and optical properties of fluorine doped tin oxide modified by ZnO nanorods and polydopamine. Chemosensors 11:106
Wang H, Zhang L, Chen Z, Hu J, Li S, Wang Z, Liu J, Wang X (2014) Semiconductor heterojunction photocatalysts: design, construction, and photocatalytic performances. Chem Soc Rev 43:5234–5244
Wang H, Zhang P, ZhigangZang Z (2020a) High performance CsPbBr 3 quantum dots photodetectors by using zinc oxide nanorods arrays as an electron-transport layer. Appl Phys Lett 116:162103
Wang H, Cao S, Yang B, Li H, Wang M, Hu X, Sun K, Zang Z (2020b) NH_4Cl-Modified ZnO for High-Performance CsPbIBr 2 Perovskite Solar Cells via Low-Temperature Process. RRL Solar 4(1):1900363
Zang Z (2018) Efficiency enhancement of ZnO/Cu_2O solar cells with well oriented and micrometer grain sized Cu_2O films. Appl Phys Lett 112:042106